



ELSEVIER

Ecological Modelling 131 (2000) 47–63

**ECOLOGICAL  
MODELLING**

www.elsevier.com/locate/ecolmodel

# Treegrass: a 3D, process-based model for simulating plant interactions in tree–grass ecosystems

G. Simioni <sup>a,\*</sup>, X. Le Roux <sup>b</sup>, J. Gignoux <sup>a</sup>, H. Sinoquet <sup>b</sup>

<sup>a</sup> *Laboratoire Fonctionnement et Evolution des Systèmes Ecologiques, Université Paris 6-CNRS-ENS, 46 rue d'Ulm, 75230 Paris, Cedex 05, France*

<sup>b</sup> *U.A. Bioclimatologie-PIAF (INRA Université Blaise Pascal), Site de Crouelle, 234 Avenue du Brézat, 63039 Clermont-Ferrand Cedex 02, France*

Received 15 September 1999; received in revised form 21 February 2000; accepted 21 February 2000

## Abstract

The function and dynamics of savanna ecosystems result from complex interactions and feedbacks between grasses and trees, involving numerous processes (i.e. competition for light, water and nutrients, fire, and herbivory). These interactions are characterised by strong relationships between vegetation structure and function. Given the heterogeneous structure of savannas, modelling appears as a convenient approach to study tree–grass interactions. Most current models that describe carbon and water fluxes are not spatially explicit, which restricts their ability to simulate plant interactions at small scales in heterogeneous ecosystems. We present here a new 3D process-based model called TREEGRASS. The model aims at predicting, in heterogeneous tree–grass systems, plant individual radiation, carbon and water fluxes at a local spatial scale. It is run at a daily time-step over periods ranging from one to a few years. The model includes (i) a 3D mechanistic submodel simulating radiation and energy (i.e. transpiration) budgets; (ii) a soil water balance submodel, and (iii) a physiologically based submodel of primary production and leaf area development. The ability of TREEGRASS to predict the seasonal courses of grass dead and leaf mass, soil water content and light regime as observed in the field has been tested for grassy and shrubby areas of Lamto savannas (Ivory Coast). Simulations showed that the spatial distribution of primary production can be strongly affected by the spatial vegetation structure. Potential applications involve predicting net primary production and water balance from the individual to the ecosystem and from the day to the annual vegetation cycle (e.g. effects of tree spatial patterns on carbon and water fluxes at the ecosystem level). © 2000 Elsevier Science B.V. All rights reserved.

*Keywords:* Savanna; Spatial patterns; Primary production; Water balance; Radiation absorption; Simulations

## 1. Introduction

Savannas are defined as ecosystems where a continuous grass layer and a discontinuous tree layer coexist (Scholes and Archer, 1997). Savanna ecosystems cover about 20% of continental sur-

\* Corresponding author. Tel.: + 33-1-44323706; fax + 33-1-44323885.

E-mail address: simioni@biologie.ens.fr (G. Simioni).

faces (Scholes and Hall, 1996) and 40% of tropical land surfaces (Solbrig et al., 1990). In addition to their highly heterogeneous vegetation structure, these ecosystems are characterised by complex interactions between tree and grass individuals that compete for light, water and nutrient resources. Being able to predict grass and tree functioning separately does not enable to predict the functioning of the coupled tree–grass system. This restricts our ability to predict tree–grass stability and dynamics in savannas (Scholes and Archer, 1997).

Assessment of tree–grass interactions has mainly been addressed by field studies. Most of them have focused on the effects of trees on the biomass and primary production of the grass layer (e.g. Knoop and Walker, 1985; Stuart-Hill and Tainton, 1989; Weltzin and Coughenour, 1990; Belsky, 1994; Mordelet and Menaut, 1995), on the soil water balance (e.g. Knoop and Walker, 1985; Joffre and Rambal, 1988; Mordelet, 1993a; Le Roux and Bariac, 1998) or on soil nutrient availability (e.g. Isichei and Muoghalu, 1992; Mordelet et al., 1993; Cruz, 1997; Rhoades, 1997). Though necessary, these studies do not point out the different processes that determine the integrated effect of one vegetation component on the other, but rather appear as a list of particular case studies.

Thus, for some authors, the only way to gain a comprehensive understanding of tree–grass coexistence and to account for the effect of vegetation structure on ecosystem physiology is to build specific models (Jeltsch et al., 1996; Scholes and Archer, 1997). During the last two decades, several modelling approaches have been proposed to simulate the functioning of tree–grass systems (Scholes and Archer, 1997). Some authors have developed models of tree–grass equilibrium that focused on the competition for soil water (Walker et al., 1981; Eagleson and Segarra, 1985). These models were generally based on a spatial segregation between grass roots exploiting mainly surface soil layers, and tree roots exploiting mainly deeper layers. More recently, simulation models predicting the effects of tree–grass interactions on grass and tree production have been developed. Among them, the GRASP model (Littleboy and McKeon,

1997) represents competition for water and nutrients, and the CENTURY-Savanna model (Parton and Scholes, unpublished), a tree–grass version of CENTURY (Parton, 1996), is based on competition for nutrients. These two models were designed to compute the bulk functioning of the tree and grass components of tree–grass systems, and use bulk information on vegetation structure (i.e. tree leaf and root biomasses or tree basal area computed at site scale) to drive tree–grass competition. The SAVANNA model (Coughenour, 1994) is a process-based model that is spatially explicit at the landscape scale (i.e. it is not individual based but each pixel is an association of one tree–grass zone and one pure grass zone). However, the choice of a relevant variable to define the respective size and dynamics of these two areas is still unclear (Coughenour, pers. comm.). To our knowledge, the only savanna model that accounts for tree individual spatial structure is the automaton model of Jeltsch et al. (1996). This model is suitable for predicting the effects of natural or man induced disturbances on tree dynamics and tree–grass equilibrium, but was not designed to study the effect of vegetation structure on water or carbon fluxes in savannas. Other modelling studies have emphasized the importance of spatial patterns (Korzukhin and Ter-Mikaelian, 1996; Pacala and Deutschman, 1995; Weishampel and Urban, 1996).

In this paper, we present a simulation model, named TREEGRASS, designed to test the effects of the fine scale vegetation structure (i.e. tree density, tree spatial distribution, crown shape and crown size distribution) on tree–grass interactions (i.e. water and carbon budgets at the site level). TREEGRASS takes into account competition for light and water in a mechanistic and spatially explicit way, and uses a biologically based approach to compute net primary production. The model is derived from three existing models: (1) the 3D RATP model (Radiation Absorption, Transpiration and Photosynthesis) (Sinoquet et al., 2000) that computes radiation and energy budgets within vegetation canopies; (2) the PEP-SEE model (Production Efficiency and Phenology in Savanna Ecosystems) (Le Roux et al., 1996) that simulates primary production and soil water

balance; (3) the MUSE simulation framework (MULTistrata Spatially Explicit model) (Gignoux et al., 1996) designed to represent an ecosystem as a set of individuals and their geometric features by a spatially explicit approach. In the next section, the TREEGRASS model is presented and is parameterised for a humid savanna ecosystem (Lamto, Ivory Coast). The ability of the model to simulate radiation absorption, primary production and soil water balance in pure grass and tree–grass areas is tested against field data. Limitations and possible applications of TREEGRASS are discussed.

## 2. The TREEGRASS model

The main original features of the 3D TREEGRASS model are that (1) trees are represented individually, (2) radial extensions of tree foliage and roots are taken into account, (3) the foliage and the root system are distributed into a grid of 3D cells, and (4) competition for light and water are treated mechanically (i.e. most relationships used are biophysical).

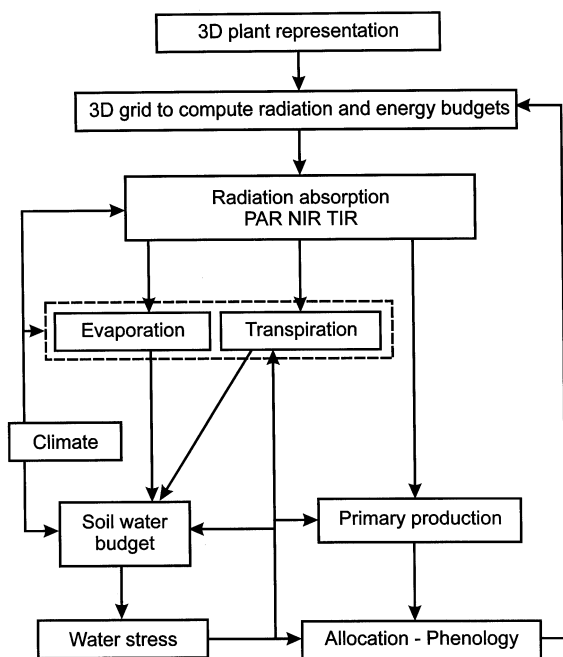


Fig. 1. Processes computed in the TREEGRASS model.

This model runs with a hourly/daily time step over one or a few vegetation cycles. The model has been developed in Borland Pascal 7. Processes considered in the model are presented in Fig. 1.

### 2.1. Main assumptions

The present version of TREEGRASS uses five major hypotheses:

1. Net primary production (NPP) is computed by the light use efficiency (LUE) approach (Monteith, 1972, 1977): one value for maximum LUE is used for trees and another value for grasses, while the same value is used for all the individuals on a site (maximum LUE values have to be determined from field measurements). The actual LUE is modulated by water stress. The assumption of the constancy of maximum LUE under different light regimes has recently been supported by the conceptual physiological model of Dewar et al. (1998).
2. The ratio of produced dry matter allocated to roots to the amount allocated to shoots is computed as a function of actual to maximum LUE values (Landsberg and Waring, 1997).
3. Over one vegetation cycle, tree architecture (crown volume and shape) is constant, and only the leaf area density (LAD) can change, tree dynamics and seedling growth are not implemented.
4. Rainfall interception by the foliage is neglected.
5. Climatic variables (wind, air temperature and humidity) are assumed to be spatially homogeneous on the site.

Nutrients, in particular nitrogen, can play an important role in tree–grass interactions (see Belsky, 1994; Scholes and Archer, 1997), but they are not explicitly treated in TREEGRASS. The present model must be considered as a first version to which a soil organic matter submodel can be coupled, in order to include the nitrogen cycle.

Two additional hypotheses were made for the simulations presented in this paper:

1. for a given simulation, only one species of grass and one species of tree are considered;

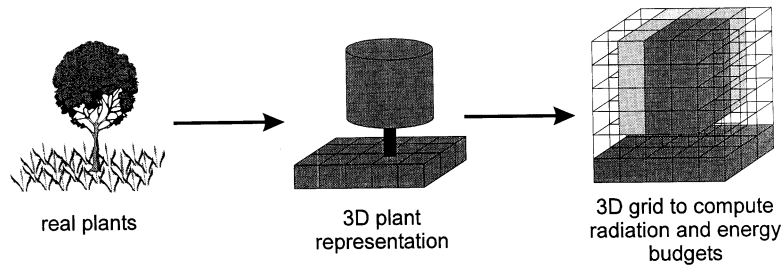


Fig. 2. Spatial representation of plants in TREEGRASS. The second picture shows the simple plant structural features used to represent trees (i.e. simple cylindrical crown, crown radius, and total height and bole height) and grasses (grass individuals are lumped into homogeneous plots and they form a continuous layer). Though they do not appear on this figure, roots are represented in a similar way. The third picture represents the 3D grid used to compute the spatial distribution of plant foliage as used by the radiation/energy budget submodel (different levels of grey correspond to different values of leaf area density (LAD)). Tree LAD is distributed using overlap coefficients between tree crown and cell volumes.

2. night transpiration is neglected (because of dew occurrence at night at the study site (Le Roux, 1995)).

### 2.2. Spatial representation of the vegetation

Plants are distributed within a 3D grid of cells (Fig. 2). The grid is divided into an above ground part, where the foliage is distributed into *vegetation cells*, and a below ground part where roots are distributed into *soil cells*. One vegetation cell can contain different types of leaves (green or dead, grass or tree, individual  $i$  or  $j$ ). In each cell, each leaf type is characterised by its LAD, inclination distribution and optical properties. Soil cells can contain roots of different plants as well.

A grass individual occupies one above ground cell and the soil cells underneath. Tree foliage and root crowns are assumed to have cylindrical shapes. Trunks and branches are not explicitly represented. Tree leaves and roots are spread into vegetation and soil cells according to overlap coefficients between cylinders and cells. Two grass ‘individuals’ (i.e. plots) do not share any vegetation nor soil cell, which is in accordance with the spatial distribution of roots observed for grasses in humid savannas (Le Provost, 1993). In contrast, a tree can share cells with grasses or with other trees. In particular, a tree compulsorily shares soil cells with grass individuals.

### 2.3. Radiation absorption

The radiation submodel has been adapted from the RATP model (Sinoquet et al., 2000). Rays from several directions are directed into the cell grid. When a ray passes through a cell, it is attenuated following Beer’s law, depending on the LAD and on the angular distribution of the vegetation entities (i.e. types of leaves) present in the cell. Intercepted radiation is shared between these entities, assuming that the leaves are randomly and uniformly distributed. Light interception by twigs and branches is neglected.

Radiation interception computed for each ray is used to calculate exchange coefficients between sources and receptors. Sky, foliage and soil are both sources (respectively of direct and diffuse radiation, and of transmitted or reflected radiation) and receptors. For one day, five representative sun directions are computed (corresponding to daytime 6:00, 9:00, 12:00, 15:00 and 18:00 h). These directions vary with the day of year and latitude. For diffuse and reflected radiation, the direction space is divided into solid angles, centered around representative heights and azimuths. Incident diffuse radiation is calculated assuming a standard overcast sky luminance distribution (Moon and Spencer, 1942). Sources of reflected radiation are calculated considering that reflection and transmission are isotropic and depend only on the angular distribution of organs. Exchange coefficients between a source and a receptor are built in

a progressive manner, adding the contribution of beams coming from the source when they meet the receptor.

These exchange coefficients are first calculated for diffuse and scattered radiation (depending thus only on the foliage characteristics and on the sky luminance distribution). For direct radiation, additional exchange coefficients are then computed for each time step, i.e. each sun direction. The first step is necessary only when the LAD of one individual has undergone a significant change. Hence, to save calculation time, exchange coefficients are computed only when a significant change in LAD (20% in our simulations) of at least one individual has occurred.

Radiation fluxes intercepted by each entity in each cell are computed by using the radiosity method (Ozsisik, 1981): the flux intercepted by a given receptor is a linear combination of fluxes coming from the whole set of sources weighed by the exchange coefficients between the sources and the receptor. Intercepted fluxes (including multiple scattering) are thus written as a system of linear equations. Solving this system allows us to calculate radiation fluxes. Details on the calculation can be found in Sinoquet and Bonhomme (1992) and in Sinoquet et al. (2000).

#### 2.4. Transpiration and evaporation

Energy budget is computed in three dimensions to determine, for each entity in each cell, the organ temperature that balances fluxes of received and lost heat:

$$Rn_{jk} - H_{jk} - E_{jk} = 0 \quad (1)$$

where  $Rn_{jk}$  is the net radiation absorbed by entity  $j$  in cell  $k$ , and  $H_{jk}$  and  $E_{jk}$  are sensible and latent heat fluxes lost by entity  $j$  in cell  $k$ . Energy budgets are established for shaded and sunny surfaces. Energy storage by the plant has been neglected. Net radiation absorption includes net balance for photosynthetically active radiation (PAR), near infra-red radiation (NIR), and thermal infra-red radiation (TIR) emitted by leaves and soil. For instance, net radiation absorption by the sunny surface  $e$  of entity  $j$  in cell  $k$  can be written:

$$Rn_{jk}^e = I_{jk}^e(\text{PAR}) + I_{jk}^e(\text{NIR}) + I_{jk}^e(\text{TIR}) - 2 \cdot \sigma \cdot (T_{jk}^e)^4 \quad (2)$$

where  $I_{jk}(\text{PAR})$  and  $I_{jk}(\text{NIR})$  are PAR and NIR fluxes calculated by the radiation absorption sub-model,  $I_{jk}(\text{TIR})$  is the TIR absorbed by entity  $j$  in cell  $k$ , and the last term represents TIR emitted by the entity surface:  $T_{jk}$  is the surface temperature of entity  $j$  in cell  $k$ , and  $\sigma$  is the Stephan–Boltzman constant ( $5.67 \cdot 10^{-8} \text{ W m}^{-2} \text{ s}^{-1} \text{ K}^{-4}$ ). Sensible heat flux can be written:

$$H_{jk}^e = \rho \cdot C_p \cdot g_b \cdot (T_{jk}^e - T_a) \quad (3)$$

where  $\rho$ ,  $C_p$ , and  $g_b$  are respectively the air density ( $\text{kg m}^{-3}$ ), the air specific heat ( $\text{J kg}^{-1} \text{ K}^{-1}$ ) and the aerodynamic conductance ( $\text{m s}^{-1}$ ) that depends on wind speed;  $T_a$  is the air temperature and  $T_{jk}^e$  is the sunny surface temperature of entity  $j$  in cell  $k$ . Similarly, the latent heat flux can be expressed as

$$E_{jk}^e = (\rho \cdot C_p / \gamma) g_w (e_{sjk}^e - e_a) \quad (4)$$

where parameters  $\gamma$  and  $g_w$  are the psychrometric constant ( $\text{Pa K}^{-1}$ ) and the leaf conductance ( $\text{m s}^{-1}$ ), respectively,  $e_{sjk}^e$  is the saturating vapour pressure at temperature  $T_{jk}^e$  estimated with the Tetens formula (1930), and  $e_a$  is the air water vapour pressure.

$g_w$  is the combination of aerodynamic and stomatal conductances of lower and upper leaf surfaces ( $g_{si}^e$  and  $g_{ss}^e$ ). These conductances depend on microclimatic factors. In this work, leaves are hypostomatous,  $g_{ss}$  is considered as nil, and the model proposed by Jarvis (1976) is used to compute  $g_{si}$ :

$$g_{si}^e = g_{smax} f_{vpd} f_{PAR} f_{SI} \quad (5)$$

where  $g_{smax}$  is the maximum stomatal conductance,  $f_{VPD}$  is a linear function for vapour pressure deficit (VPD),  $f_{PAR}$  is a nonlinear function of PAR (Jarvis, 1976), and  $f_{SI}$  is a threshold function accounting for water stress (SI is the stress index, see Section 2.5.3).

Similarly, an energy budget for each soil cell of the upper layer is calculated taking into account a conductive heat flux  $G$  into the soil:

$$Rn_{ks} - G_{ks} = E_{ks} + H_{ks} \quad (6)$$

where  $G_{ks}$  is calculated as a fraction of  $Rn_{ks}$  in soil cell  $ks$ , according to vegetation phenology (Le

Roux, 1995). As for leaves, solving the soil energy budget requires the determination of the soil aerodynamic resistance and the soil surface resistance to water vapour transfer. The former depends on wind speed while the latter depends empirically on the quantity of water evaporated since last rain in soil upper layer (Amadou, 1994).

The overall energy budget for sunny and shaded surfaces of each entity  $j$  in each cell  $k$  (including soil cells) makes an equation system in which surface temperatures are the unknowns. The energy budget is solved using the Newton–Raphson algorithm by successive iterations. Further details are given by Sinoquet et al. (2000).

Evaporation, transpiration and absorbed PAR obtained for each entity in each cell are summed up to calculate daily soil evaporation, and individual plant transpiration and absorbed PAR.

## 2.5. Soil water budget

Soil is divided into two strata, an upper layer (layer 1, the depth of which is defined so that this layer includes 90% of the grass roots), the layer 2 (down to the maximum plant rooting depth), plus the deep soil underneath.

### 2.5.1. Soil water extraction

Water evaporated is extracted from the soil upper layer cells. Water transpired by each individual is extracted from the soil cells occupied by the plant roots, using overlap coefficients between volumes of soil occupied by roots and soil cell volumes. The total transpiration  $T$  is extracted from layer 1 ( $T_1$ ) and from layer 2 ( $T_2$ ) for an individual; values for  $T_1$  and  $T_2$  depend on the water stress index and are calculated as:

$$T_1/T = (T_1/T)_{\max} f_{SI} \quad (7a)$$

$$T_2 = T - T_1 \quad (7b)$$

where  $(T_1/T)_{\max}$  is a species specific parameter, the fraction of the plant total transpiration extracted in layer 1 under non-limiting water conditions. Transpired water that can't be extracted from layer 1 or 2, because their wilting points are reached, is assumed to be taken up from the deep soil.

### 2.5.2. Run-off and drainage

Run-off occurs if precipitation  $P$  exceeds a threshold value  $P_0$  and if the total LAI is below a threshold value LAI<sub>0</sub> (De Jong, 1983):

$$\text{RunOff} = a(P - P_0) \quad (8)$$

where  $a$  is an empirical parameter.

Drainage (from layer 1 to layer 2, and from layer 2 to deep soil) is computed by a simple bucket model (i.e. drainage occurs when the soil water content of a given layer exceeds field capacity).

### 2.5.3. Water stress

In the model, for each plant, the stress index depends on the soil water content in layer 1, as Le Roux and Bariac (1998) found that water potentials of *Crossopteryx febrifuga*, a tree species, and *Hypparrhenia diplandra*, a grass species, were related with water potential in the 0–60 cm soil horizon. Each soil cell in layer 1 has a corresponding stress index:

$$R_1 \leq R_{l1} \quad f_{SI} = (R_1 - R_{wp1}) / (R_{l1} - R_{wp1}) \quad (9)$$

$$R_1 > R_{l1} \quad f_{SI} = 1$$

where  $R_1$  and  $R_{l1}$  are the actual and threshold values of soil water content in layer 1, and  $R_{wp1}$  is the soil water content of layer 1 at wilting point.

In layer 1, a grass individual has its roots in only one cell, its water stress index is thus determined by the water content of this cell. On the opposite, the stress index for a tree individual is a combination of the stress indices of the different cells where its roots are present. All soil cells occupied by roots of a given tree contribute to its stress index in proportion to overlaps between the root crown volume and cell volumes.

## 2.6. Primary production and allocation

### 2.6.1. Fire

Fire occurs at a prescribed date, according to field observations. To avoid to model the kinetics of the allocation from roots to shoots after fire for grasses (Le Roux et al., 1997), leaf biomass is initialised to a minimum value ( $10 \text{ g m}^{-2}$ ), as proposed by Ciret et al. (1999). In a similar way, fire reduces individual tree LAI to 0.1 (on a projected crown area basis).

### 2.6.2. Dry matter production

The light use efficiency approach (Monteith, 1972 and Monteith, 1977) is applied to each grass:

$$\text{TNPP} = E_b \cdot \text{APAR} \quad (10)$$

where TNPP is the total net primary production of the individual ( $\text{g unit time}^{-1}$ ), APAR is the PAR absorbed by the plant ( $\text{MJ unit time}^{-1}$ ), and  $E_b$  is the conversion efficiency of APAR into dry matter ( $\text{g MJ}^{-1}$  APAR).  $E_b$  is given by:

$$E_b = E_{b\text{max}} \cdot f_{\text{SI}} \quad (11)$$

where  $E_{b\text{max}}$  is the maximum conversion efficiency (i.e. without water stress). One value of  $E_{b\text{max}}$  is used for trees and one for grasses.

### 2.6.3. Allocation

The proportion of TNPP allocated to shoots ( $\eta_s$ ) is given by the empirical relation proposed by Landsberg and Waring (1997):

$$\eta_s = 1 - (\alpha / (1 + \beta (E_b / E_{b\text{max}}))) \quad (12)$$

For example, with  $\alpha = 0.6$  and  $\beta = 0.5$ , a plant allocates 60% of carbon to shoots when  $E_b / E_{b\text{max}}$  and thus  $f_{\text{SI}} = 1$ . This fraction decreases to 40% when the water stress is maximum (and when production tends to zero). Such an effect of drought on root/shoot allocation has been reported in field studies (e.g. Durand et al., 1989) and is in accordance with the functional equilibrium theory (Brouwer, 1983). For trees, a similar approach is used to compute root/shoot allocation.

In addition, because tree above ground production is shared between leaves and branches/trunk, we assume that all the above ground growth is allocated to leaves as long as the plant has not reached its maximum LAI (each tree is given a maximum LAI value related to its size, see Section 3.1.2).

### 2.6.4. Seasonal variations in biomass and necromass

For each grass individual, variations in biomass and necromass compartments are computed as (Le Roux, 1995):

$$B_t = B_{t-1}(1 - \Gamma_M) + \text{TNPP}\eta_s \quad (13a)$$

$$N_t = N_{t-1}(1 - \Gamma_D) + B_{t-1}\Gamma_M \quad (13b)$$

$$R_t = R_{t-1}(1 - \Gamma_R) + \text{TNPP}(1 - \eta_s) \quad (13c)$$

where  $B$  and  $N$  are above ground biomass and necromass ( $\text{g m}^{-2}$ ),  $\Gamma_M$  and  $\Gamma_D$  are above ground mortality and decomposition rates ( $\text{g g}^{-1} \text{day}^{-1}$ ), and  $t$  is time (days). Because of the lack of mortality and decomposition data for roots in savannas, the root compartment is represented simply by a phytomass  $R$  ( $\text{g m}^{-2}$ ) with a constant decomposition rate  $\Gamma_R$  ( $\text{g g}^{-1} \text{day}^{-1}$ ). For each tree individual, variations in the leaf biomass  $B$ , are given by ( $\text{LAI}_{\text{max}}$  is the maximum tree LAI):

if  $\text{LAI} < \text{LAI}_{\text{max}}$  (before the dry season):

$$B_{it} = B_{it-1}(1 - \Gamma_M) + \text{TNPP}\eta_s \quad (14a)$$

$$\text{else: } B_{it} = B_{it-1}(1 - \Gamma_M) \quad (14b)$$

For grasses, above ground mortality and decomposition rates are assumed to be zero after fire until grass individual LAI reaches 1, and constant afterwards (Le Roux, 1995). For tree individuals, the leaf mortality rate is nil before the dry season, and depends on water stress during the dry season

$$\Gamma_M = \chi(1 - f_{\text{SI}}) \quad (15)$$

where  $\chi$  is the maximal mortality rate. Tree leaf fall is assumed to be instantaneous, i.e. there is no dead leaf accumulation within the tree foliage (Mordelet, 1993a). All the remaining green leaves fall after fire occurrence (Menaut, 1974).

Grass green LAI is computed according to specific leaf area values decreasing with increasing grass biomass values. A constant specific leaf area is used for grass dead leaves and tree green leaves (Le Roux, 1995).

## 3. Application of TREEGRASS to the Lamto savannas

### 3.1. Parameterisation of the model

The model has been parameterised for the humid savanna of Lamto, Ivory Coast (Menaut and César, 1979) (Table 1).

Table 1

Sources and values of the TREEGRASS model parameters used for simulations of Lamto savannas

Parameters	Values	References
<i>Radiation profile</i>		
PAR/global radiation ratio	48	Le Roux et al., 1997
Diffuse/global radiation ratio	60	Gauthier, 1993
Atmospheric radiation ( $W m^{-2}$ )	350	Le Roux, 1995
<i>Leaf angular distribution</i>		
Grass living leaves	erectophile	Le Roux et al., 1997
Grass dead leaves	planophile	Id.
Tree	spherical	NA <sup>a</sup>
<i>PAR absorbances</i>		
Ground	0.76	Le Roux et al., 1997
Grass living leaves	0.78	Id.
Grass dead leaves	0.35	Id.
Tree	0.78	NA <sup>a</sup>
<i>PIR absorbances</i>		
Ground	0.50	Le Roux et al., 1997
Grass living leaves	0.04	Id.
Grass dead leaves	0.05	Id.
Tree	0.10	NA <sup>a</sup>
<i>Soil layer depths (cm)</i>		
Layer 1	60	Le Roux, 1995
Layer 2	110	Id.
<i>Soil water contents (mm)</i>		
Layer 1 field capacity	104.6	Le Roux and Bariac, 1998
Layer 1 threshold (RI1)	60	Id.
Layer 1 wilting point (Rwp1)	30.9	Id.
Layer 2 field capacity	187	Id.
Layer 2 wilting point	100	Le Roux, unpublished
<i>Run-off</i>		
Minimum precipitation ( $P_0$ , mm)	22	De Jong, 1983
Maximum LAI ( $LAI_0$ )	2.5	Id.
A	0.1394	Id.
<i>Maximum stomatal conductances <math>g_{smax}</math> (<math>mmol m^{-2}s^{-1}</math>)</i>		
Grass	230	Sueur, 1995
Tree	230	NA <sup>a</sup>
<i>Maximum fraction of transpired water extracted from layer 1 (<math>T1/T</math>)<sub>max</sub></i>		
Grass	0.9	Le Roux, 1995
Trees	0.7	Le Roux et al., 1995
Grass	1.14	Le Roux et al., 1997
Tree	0.8	Bégué, pers. com.
<i>Fraction of production allocated to above ground parts (for trees and grass) (%)</i>		
Without water stress	60	Durand et al., 1989
With water stress (minimum value)	40	Id.
<i>Initialisations after fire</i>		
Grass leaf biomass ( $g m^{-2}$ )	10	Ciret et al., 1999
Tree individual LAI	0.1	Arbitrary
<i>Others</i>		
Grass mortality rate $\Gamma_M$ ( $d^{-1}$ )	0.012	Le Roux, 1995
Grass decomposition rate $\Gamma_D$ ( $d^{-1}$ )	0.015	Id.
Grass phytomass decomposition rate $\Gamma_R$ ( $d^{-1}$ )	0.002	Id.
Grass dead specific leaf area ( $cm^2 g^{-1}$ )	144	Id.
Tree maximum leaf mortality rate $\zeta$ ( $d^{-1}$ )	0.04	NA <sup>a</sup>
Tree specific leaf area ( $cm^2 g^{-1}$ )	90	Gauthier, 1993; Medina, 1982; Medina and Francisco, 1994

<sup>a</sup> NA; Not available.

### 3.1.1. Climatic data

Daily global radiation, rainfall and wind speed, and daily courses of air temperature and VPD measured at Lamto in 1991–1992 (Le Roux, 1995) were used as input variables. A sinusoidal evolution of global radiation was assumed during the day, sampled at five sun positions. PAR was considered as a fixed amount of global radiation (48%) (Le Roux et al., 1997). Because the amount of diffuse radiation has not been routinely recorded at Lamto, it was assumed constant and equal to 60% of global radiation (Gauthier, 1993). Atmospheric radiation was also assumed to be constant and equal to  $350 \text{ W m}^{-2}$  according to measurements made at Lamto in 1991–1992. Wind speed was assumed constant throughout the day. For each day, the model used five temperature and VPD values (recorded in 1991–1992) corresponding to the five sun directions used.

### 3.1.2. Plant data

The  $C_4$  perennial bunch grass species considered here was *Hyparrhenia* spp. (Andropogoneae). The tree type corresponded to a dominant, deciduous, shallow-rooted species present at Lamto: *Crossopteryx febrifuga*.

Each tree was characterised by its location (spatial position of the trunk), its total height ( $Ht$ , in meters), and cylindrical leaf and root crown shapes. The basal leaf crown surface (i.e. tree foliage projected crown surface;  $CS$ , in  $\text{m}^2$ ) was given as (Gignoux, regression based on unpublished data):

$$CS = 0.4372 \cdot Ht^{1.7228} \quad (16)$$

Bole height was assumed to be half of  $Ht$ . Root crown radius (RCR) depended on the leaf crown radius (RC) (Mordelet, 1993a):

$$RCR = 1.5 \cdot RC \quad (17)$$

Maximum tree LAI was determined from  $CS$  as (Menaut, unpublished):

$$LAI_{\max} = 0.65 \cdot CS^{1.065} \quad (18)$$

Tree architecture was assumed to be fixed (i.e. there was no crown volume variation during a vegetation cycle). Grass green (LAI) and dead

(dLAI) leaf area indices were computed from biomass  $B$  and necromass  $N$  according to measured specific green and dead leaf areas (Le Roux, 1995):

$$LAI = (128 - 62(1 - e^{-0.0102 \cdot B}))B \cdot 10^{-4} \quad (19a)$$

$$dLAI = 0.0144 \cdot N \quad (19b)$$

Tree specific leaf area (SLA, Table 1) has been measured by Gauthier (1993). Possible temporal evolution of tree SLA was neglected.

Published values of stomatal conductance for *Hyparrhenia* spp. under sub-optimal conditions ranged from 202 to 296  $\text{mmol m}^{-2} \text{s}^{-1}$  (Simoes and Baruch, 1991) or from 120 to 275  $\text{mmol m}^{-2} \text{s}^{-1}$  (Sueur, 1995). A maximal stomatal conductance of 230  $\text{mmol m}^{-2} \text{s}^{-1}$  was used for the simulations. Very few stomatal conductances have been reported for savanna trees (see Schulze, 1994). Ullman (1985) observed maximal values up to 220  $\text{mmol m}^{-2} \text{s}^{-1}$  for different acacia species in sahelian and saharian zones. Schulze (1994) gave values for different vegetation types: 145  $\text{mmol m}^{-2} \text{s}^{-1}$  for monsoonal forests, 200 for sclerophyllous shrubland, 190 for temperate deciduous trees, 273 for tropical deciduous forests, and 207 for tropical rainforests. In the present study, we chose a maximum stomatal conductance of 230  $\text{mmol m}^{-2} \text{s}^{-1}$  for trees.

Values for  $f_{\text{VPD}}$  and for  $f_{\text{PAR}}$  were computed as:

$$\text{For grass (Baruch et al., 1985),} \\ f_{\text{VPD}} = 1.25 - 2.5 \cdot 10^{-4} \cdot \text{VPD} \quad (20a)$$

$$\text{For trees (Le Roux et al., 1999),} \\ f_{\text{VPD}} = 1.18 - 1.8 \cdot 10^{-4} \cdot \text{VPD} \quad (20b)$$

$$\text{(Le Roux et al., 1999)} \\ f_{\text{PAR}} = 0.030978 \cdot \text{APAR} / (1 + 0.030978 \cdot \text{APAR}) \quad (21)$$

where VPD is the vapour pressure deficit (Pa) and APAR is the absorbed PAR for a given sun position.

Above ground maximal conversion efficiency has been measured at Lamto for grass (Le Roux et al., 1997), and in a dry savanna in West Africa for trees (Bégué, personal communication) (Table 1).  $E_{\text{bmax}}$  values were assumed to be twice the

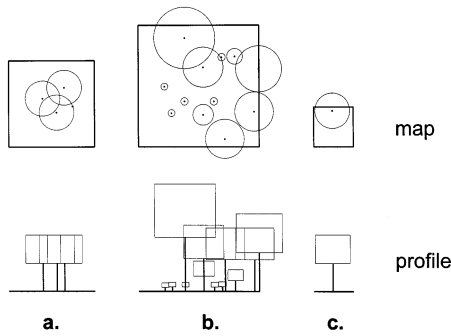


Fig. 3. Tree-grass plots used to test the model. Tree trunks (dots and bars) and canopies (circles and rectangles) are represented. (a) Tree clump site (6 × 6 m). (b) Site corresponding to Gauthier's study (1993), rebuilt from tree structure data (8 × 8 m). (c) Site used to test the effects of cell dimensions (30 m). Trees in sites (a) and (c) were identical (3.61 m high, canopy area of 4 m<sup>2</sup>).

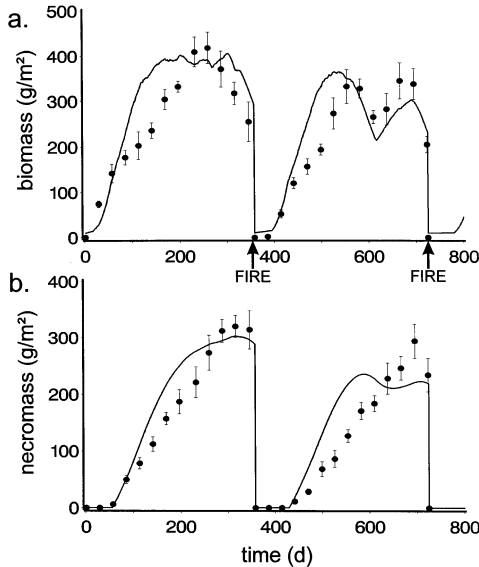


Fig. 4. Measured (•) (Le Roux, 1995) and simulated (lines) seasonal courses of grass above ground biomass (a) and necromass (b) in an open (pure grass) site, during two annual vegetation cycles. Bars represent one standard deviation.

measured values of above ground maximal conversion efficiency (i.e. assuming a root:shoot ratio of 1 for production). Grass conversion efficiency was supposed to be constant under tree cover and in open areas. This is consistent with Cruz's results (Cruz, 1997) which showed that conversion efficiency did not differ under or out of tree cover for *Dichanthium aristatum*, a C<sub>4</sub> tropical grass species.

Allocation parameters in Eq. (12) were chosen so that plant allocated 60% of their assimilates to above ground parts without water stress and 40% with maximum water stress (Table 1).

### 3.1.3. Data for soil water storage and water flow

Values of soil water contents in layers 1 and 2 at field capacity and wilting point were estimated from field observations (Table 1). Aerodynamic soil resistance was prescribed. Soil surface resistance to water vapour transfer (SSR) depended on the amount of water evaporated since last rainfall from layer 1 ( $E_{cum}$ ) (Amadou, 1994):

$$SSR = 80 \cdot e^{0.23 \cdot E_{cum}} \quad (22)$$

The conductive heat flux  $G$  in the soil was a constant fraction of net radiation ( $Rn$ ) of the soil grass system (Le Roux, 1995)

$$G_{ks}/Rn_{ks} = 0.3 - 0.22 \cdot C_{ks} \quad (23a)$$

$$C_{ks} = 1 - e^{-0.607 \cdot LAI} \quad (23b)$$

where  $C_{ks}$  is the grass fractional cover over the soil cell  $ks$ .

According to Le Roux (1995), under non-limiting water conditions, grasses took up 90% of transpired water from layer 1 (i.e. transpiration fraction extracted from layer 1  $(T_1/T)_{max} = 0.9$ ). The ratio  $(T_1/T)_{max}$  is 0.7 for trees (Le Roux and Bariac, 1998). Field data also showed that water stress should be calculated from water content in layer 1 for both grasses and trees (Le Roux and Bariac, 1998).

Runoff was computed when threshold values for daily precipitation ( $P_0 = 22\text{mm}$ ) and LAI ( $LAI_0 = 2.5$ , including grass dead LAI) were reached, as observed by De Jong (1983) at Lamto.

### 3.2. Simulations performed

The model was tested by comparing its outputs with measured data. Simulations were performed using:

1. a pure grass site (i.e. one grass individual) for which TREEGRASS outputs of seasonal dynamics of grass above ground biomass and necromass, and seasonal courses of soil water contents in layers 1 and 2 were tested against 1991–1992 field data from Le Roux (1995);

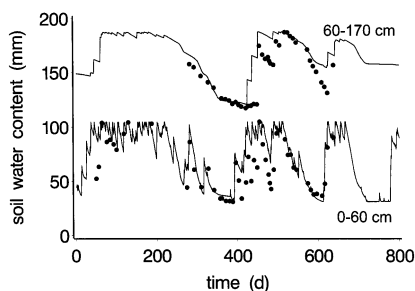


Fig. 5. Measured (\*) (Le Roux, 1995) and simulated (lines) seasonal courses of soil water contents in the two upper layers (0–60 cm and 60–170 cm) in an open (pure grass) site, during two annual vegetation cycles.

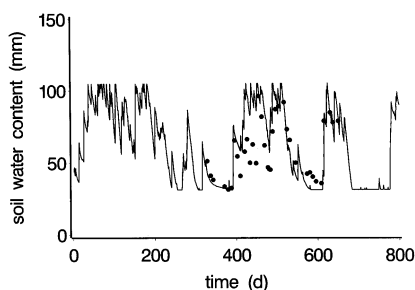


Fig. 6. Measured (\*) (Le Roux, 1995) and simulated (line) seasonal courses of soil water content in the upper layer (0–60 cm) under a tree clump, during two annual vegetation cycles.

2. a tree clump site (a  $6 \times 6$  m site with a clump of three trees at the center, see Fig. 3a) for which TREEGRASS outputs of the seasonal course of soil water content in layer 1 under tree cover were tested against 1991–92 field data from Le Roux (1995) (Fig. 4);
3. a tree–grass site corresponding to the site where radiation absorption was studied at Lamto (Fig. 3b) for which TREEGRASS outputs of tree radiation absorption were tested against field data from Gauthier (1993).

For each test, the model was run using climatic data measured in 1991–1992. Cell basal dimensions were  $1 \times 1$  m (cell basal dimensions refers to the side length of the square basis of a cell). In addition, and in order to assess possible effects of cell basal dimensions, simulations were carried out with the tree–grass site of Fig. 3(c) using different cell sizes. Finally, in order to illustrate possible

effects of the tree spatial structure on spatial production patterns, two other simulations were conducted with distinct tree spatial distributions.

## 4. Results

### 4.1. Pure grass site

Although the model slightly overestimated primary production at the beginning of each cycle, the seasonal dynamics of biomass and necromass were adequately simulated (Fig. 4). The water stress effect in the middle of the 1992 vegetation cycle was satisfactorily simulated. Over the two years, measured and simulated biomasses and necromasses were well correlated ( $R^2 = 0.83$ ,  $F_{1,26} = 130.6$ ,  $P = 0.0001$  for biomass; and  $R^2 = 0.88$ ,  $F_{1,26} = 193.2$ ,  $P = 0.0001$  for necromass). The seasonal courses of soil water contents in layers 1 and 2 were also adequately simulated by the model (Fig. 5). Measured and simulated soil water contents were well correlated ( $R^2 = 0.64$ ,  $F_{1,37} = 66.6$ ,  $P = 0.0001$  for layer 1, and  $R^2 = 0.75$ ,  $F_{1,37} = 113.3$ ,  $P = 0.0001$  for layer 2). Nonetheless, soil water content in layer 1 was overestimated at the beginning of the vegetation cycle and early drainage was thus simulated from layer 1 to layer 2 around day 425.

Mean values of annual above ground and total NPP computed by TREEGRASS, using 1991–1992 climatic data, were  $15.3 \text{ t ha}^{-1}$  and  $25.8 \text{ t ha}^{-1}$ , respectively. These numbers were close to values reported for Larrito savannas:  $12.7 \text{ t ha}^{-1}$  for above ground NPP (Le Roux, 1995),  $9.6 \text{ t ha}^{-1}$  for below ground NPP (Abbadie, 1983), and from  $21.5$  to  $35.8 \text{ t ha}^{-1}$  for total NPP in savanna grasslands (Menaut and César, 1979).

### 4.2. Tree clump site

Measured and simulated soil water contents under tree clump were well correlated ( $R^2 = 0.68$ ,  $F_{1,34} = 73.4$ ,  $P = 0.0001$ ), despite an overestimation at the beginning of the vegetation cycle (Fig. 6).

Simulated grass above ground NPP under tree clump corresponded to 45% of the above ground

NPP in open areas (not shown). Simulated grass above ground NPP under tree clump was therefore slightly lower than that observed by Mordelet and Menaut (1995) who reported a value of 63%.

#### 4.3. PAR absorption by trees

Fig. 7 shows the PAR absorption efficiency of trees in relation to tree total LAI. For low tree LAI (under 0.4), the model, which does not account for PAR absorption by woody parts, underestimated tree PAR absorption efficiency. Above a tree LAI of 0.4, tree PAR absorption efficiency was correctly simulated. The model gave sets of different tree LAI for which PAR absorption efficiencies were identical. This is because, as reported earlier in the model description, new LAI values are used in the radiation absorption submodel only if, for at least one plant, a change of 20% has been reached. For a given value of tree LAI, there were also different values of tree PAR absorption efficiencies because the simulation was done for two vegetation cycles, and in each cycle, tree LAI increased and decreased (leaves expanded and fell). The tree LAI threshold of 0.4 was reached between two to three months after fire occurrence, depending on the year.

#### 4.4. Effects of cell basal dimensions

Compared to PAR absorption efficiency or water fluxes, NPP was the most sensitive variable to cell basal dimensions. Total grass NPP increased from 12.79 to 14.34 t ha<sup>-1</sup> (12.1% variation)

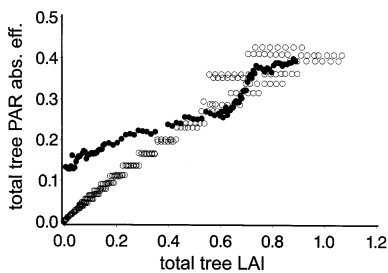


Fig. 7. Measured (\*) (Gauthier, 1993) and simulated (o) total tree PAR absorption efficiency as a function of total tree LAI.

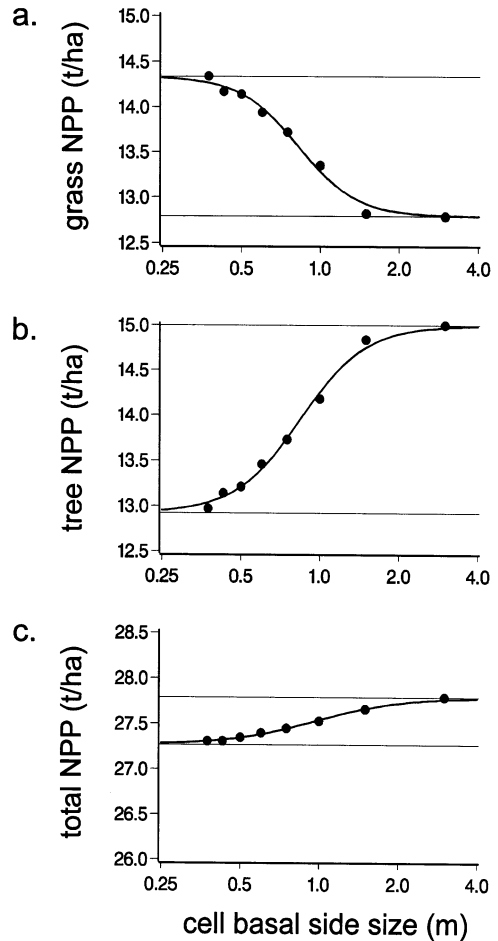


Fig. 8. Effects of cell basal dimensions on (a) grass; (b) tree and (c) total net primary productions simulated over one vegetation cycle (1991). Logarithmic scale is used for cell basal side size. Dots represent simulations, thick lines represent non linear regressions and thin lines are regression asymptots. All figures are at the same scale.

when cell basal side size decreased from 3 to 0.375 m, respectively (Fig. 8a). On the opposite, total tree NPP decreased from 15.00 to 12.97 t ha<sup>-1</sup> (13.5% variation) (Fig. 8b). Total NPP decreased little with decreasing cell basal dimensions (1.7% variation) (Fig. 8c). Thus changing cell basal dimensions affected primarily the NPP distribution between the grass and tree components more than the overall production.

In the case of a cell size of 30 m, as whole site dimensions were 3 × 3 m, the system was homoge-

neous (i.e. one grass layer fully overlapped by one tree layer). When cell size decreases, one can expect model outputs to reach an asymptotic state as the model approaches a cell size of zero (i.e. a continuous description of space). We fitted a logistic curve through non linear regression (PROC NLIN, SAS Institute, 1990) to NPP values as a function of  $\log(\text{cell basal side size})$ . Values of NPP obtained for the maximal cell size (30 m) were used as asymptotes for the logistic curves (i.e. top asymptotes for total and tree NPP, basal asymptote for grass NPP). The nonlinear fit algorithm converged in all cases and gave the following estimates for asymptotes corresponding to a cell size decreasing towards zero:  $14.33 \text{ t ha}^{-1}$  for grass NPP (corrected  $R^2 = 0.99$ ,  $F_{3,5} = 8097636$ ,  $P < 0.0001$ ),  $12.92 \text{ t ha}^{-1}$  for trees (corrected  $R^2 = 0.99$ ,  $F_{3,5} = 107726$ ,  $P < 0.0001$ ) and  $27.25 \text{ t ha}^{-1}$  for the total system (corrected  $R^2 = 0.99$ ,  $F_{3,5} = 93992$ ,  $P < 0.0001$ ). These values are closed to those simulated with a cell size of  $0.375 \times 0.375 \text{ m}$ .

#### 4.5. Spatial patterns of NPP affected by tree spatial distribution

Fig. 9 presents the effects of tree spatial distribution on grass NPP spatial heterogeneity. Overall

grass production with aggregated trees ( $17.66 \text{ t ha}^{-1}$ ) was 20% higher than with randomly distributed trees ( $14.43 \text{ t ha}^{-1}$ ). When trees were randomly located (Fig. 9a) 93% of the site surface showed a grass NPP between 900 and  $2100 \text{ g m}^{-2}$ . When trees were aggregated (Fig. 9), high grass productions were more frequent: 67% of the surface showed a grass NPP above  $1700 \text{ g m}^{-2}$ . Thus both grass NPP spatial distribution and mean values at the site scale were strongly influenced by tree spatial structure.

## 5. Discussion

The RATP model and its ability to simulate the distribution of light regime, carbon acquisition and transpiration within plant foliage had already been tested by its authors (Sinoquet et al., 2000). The radiation absorption submodel ability to reproduce grass radiation absorption had also been tested for a savanna grassland at Lamto (Le Roux et al., 1997). The production/water balance module of PEPSEE had been tested for savanna grasslands as well (Le Roux et al., 1996).

Our results showed that the model simulated quite accurately radiation, carbon and water pro-

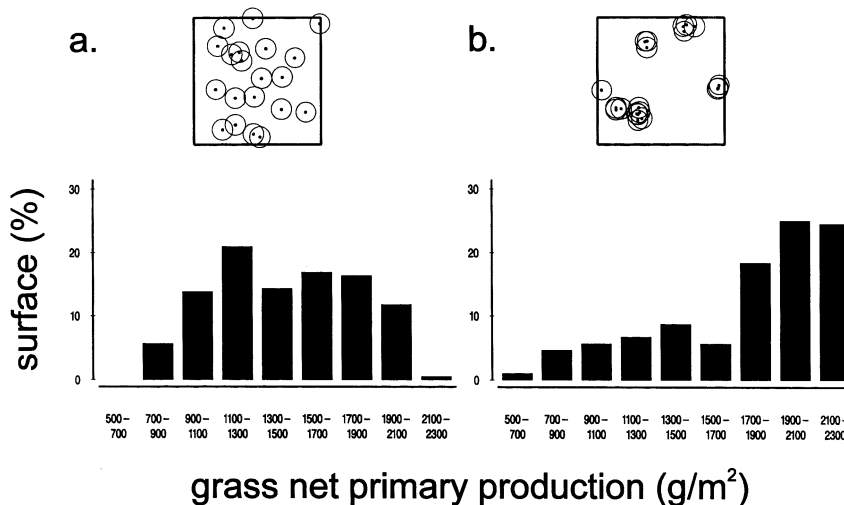


Fig. 9. Differences in the simulated spatial distribution of grass net primary production over one vegetation cycle when trees are (a) randomly distributed or (b) highly aggregated. Plots above graphs show the sites used for simulations ( $14 \times 14 \text{ m}$ ), with their tree spatial distributions. Tree number is 20 and all trees are identical (3.61 m high, canopy area of  $4 \text{ m}^2$ ).

cesses. These tests were done with integrative variables (biomass, radiation absorption, soil water contents, NPP) involving the whole or at least a large part of the processes implemented in the model. In addition, simulations were done using different sites with varying tree spatial structure, making use of available field data for the Lamto savannas. Hence, TREEGRASS appears able to simulate the effects of vegetation structure on NPP and water balance of Lamto savannas, despite the absence of nutrients and rainfall interception, and a simple tree architecture. However, these results also showed that the TREEGRASS model has some limits.

### 5.1. Plant radiation absorption

Tree PAR absorption efficiency was correctly simulated, except at the beginning of cycle, for low tree LAI, probably because stems and branches were not represented in the model. In the field, these organs are able to absorb some radiation when leaves are not fully expanded. Jackson et al. (1990) reported a radiation interception efficiency of 0.25 for deciduous oaks without leaves. Stem material of numerous Texas savanna tree species showed a strong absorbance in a PAR spectral range, so that stem surfaces may have increased canopy PAR absorption efficiency by 10–40% when tree LAI was low (Asner et al., 1998). This could be implemented in the model if reliable and simple data were available on tree architecture in Lamto savannas. Anyway, it was not a major problem in our simulations as radiation absorbed by branches would not have been converted into dry matter, though stems could alter the spatial distribution of radiation absorption. When tree LAI is sufficiently high, this problem can be neglected.

A previous work showed that the radiation absorption submodel had a tendency to overestimate grass PAR absorption at the beginning of the vegetation cycle (data not shown but see Le Roux et al., 1997). This was potentially due to the fact that the grass stratum was assumed to be continuous throughout the year, although the grass layer is composed of tufts that do not fully cover the soil during the first two months of the

cycle. The importance of the grass fractional cover could be tested on a pure grass site, by explicitly taking into account grass spatial development at the beginning of the cycle.

### 5.2. Carbon processes

This overestimation of the grass PAR absorption entailed an overestimation of grass production at the beginning of each cycle (Fig. 4).

The simulated reduction of grass NPP under tree clump was slightly higher than that observed in the field, this could be due to the fact that the model did not treat nutrients, as higher nutrient availability is expected under tree cover (Mordelet et al., 1993). As already mentioned, we plan to add nutrient processes in TREEGRASS.

### 5.3. Water processes

The overestimation of the grass radiation absorption could also be responsible for an underestimation of soil evaporation at the beginning of the vegetation cycle. This effect could explain why TREEGRASS overestimated the soil water content in layer 1 at the beginning of each cycle. Other reasons for this overestimation could be a possible different soil albedo after fire with the presence of ash during 1 to 3 weeks (Le Roux et al., 1994), and a change in the soil surface status at the end of the dry season that would have increased the runoff. These two possibilities were not computed, sensitivity analyses are needed to test these hypotheses.

The seasonal course of water content in soil layer 2 under a tree clump was not tested because of lack of data. For the same reason, the partitioning of evapotranspiration between evaporation, grass and tree transpiration rates could not be tested. It is clear that it would be interesting to test the model ability to simulate the evaporation rate according to the tree spatial distribution, and the relative importance of tree and grass transpiration rates. In particular, comparing the simulated tree transpiration with measured sap flow rates (e.g. Howard et al., 1997) is needed. Grass transpiration is more difficult to measure: using gas exchange chambers (Tournebize et al., 1996),

for instance, can alter the microclimate experienced by grasses.

Finally, it appeared that, despite of the absence of rainfall interception by the foliage, the model correctly simulated the grass behaviour in the absence of trees. A few data are available for rainfall interception by grass at Lamto and could be used to include this process in the model.

#### 5.4. Importance of the size of grid cells

The smaller the cell size, the more accurate the representation of the tree crown shape, and the more accurate the simulation of competition for light. The ideal size would be the one under which there is no variation (in NPP for instance). The smallest cell size that a computer could handle for the tests was  $0.375 \times 0.375$  m, and it seems that, from the non linear regression fit, it was very close to the ideal cell size. For larger sites, like those presented in Fig. 9, with sizes compatible with the scale of an ecosystem study, the cell size limit for computers became  $1 \times 1$  m. This was applied to all test simulations as an acceptable compromise between precision and computer requirements. This does not mean that plots used for simulations should be small. The maximum plot size depends mainly on the type of vegetation: the denser the vegetation, the higher the number of vegetation cells, and the longer the simulations.

#### 5.5. Spatial heterogeneity of grass NPP and tree spatial distribution

Due to their size, trees have first access to light. When trees were aggregated, there were larger open areas, i.e. more grass surface where there was no or little tree influence. These open areas showed a high grass NPP. On the opposite, a random distribution was associated with more isolated trees, and thus entailed stronger interactions between trees and grasses. These results emphasize the interest to study effects of the vegetation spatial structure on radiation, carbon, and water fluxes. Knowing when fine tree spatial structure needs to be considered for the functioning of an ecosystem is one important purpose of TREEGRASS.

## 6. Conclusion

Tests described in this paper and using a  $1 \times 1$  m resolution were conclusive:

1. Seasonal variations in biomass, necromass and soil water contents in layers 1 and 2 were satisfactorily simulated by the model in the case of a pure grass site.
2. Primary production values computed by the model were consistent with values reported in the literature.
3. The model correctly simulated the seasonal course of the soil water content in layer 1 under tree clump.
4. Tree PAR absorption efficiency was also correctly simulated.

As already mentioned, the model described in this paper must be considered as a first version. In the near future, we plan to add mechanistic computations for nitrogen processes, photosynthesis and a better tree architecture, in order to build a complete mechanistic model able to simulate daily savanna functioning. Breshears et al. (1997) found that, in New Mexico semiarid woodlands, two different tree species exploited soil water differently. A similar conclusion was raised by Le Roux and Bariac (1998) at Lamto. Other studies showed that grass species composition can be different under tree cover or in open areas (e.g. Belsky et al., 1993; Scholes and Archer, 1997). Thus, it appears necessary to introduce more species in our simulations, in order to account for functional diversity.

In the near future, TREEGRASS will be used to assess (1) the influence of tree spatial structure on total carbon and water fluxes at the site level (which is currently under progress); (2) the spatial and temporal distributions of production and water fluxes between individuals; (3) the effects of different tree types (e.g. deciduous versus evergreen, deep-rooted versus shallow rooted) on tree–grass interactions.

## Acknowledgements

This work was supported by the European Terrestrial Ecosystem Modelling Activity (ETEMA) and by the Programme National de Recherche en

Hydrologie (grant 99-PNRH 14, publication # 189).

## References

- Abbadie, L., 1983. Aspects fonctionnels du cycle de l'azote dans la strate herbacée de la savanne de Lamto. Ph.D. Thesis, University Paris, pp. 158.
- Amadou, M., 1994. Analyse et modélisation de l'évapotranspiration d'une culture de mil en région sahélienne. Ph.D. Thesis, University Paris, pp. 106.
- Asner, G.P., Wessman, C.A., Archer, S., 1998. Scale dependence of absorption of photosynthetically active radiation in terrestrial ecosystems. *Ecol. Appl.* 8, 1003–1021.
- Baruch, Z., Ludlow, M.M., Davis, R., 1985. Photosynthetic responses of native and introduced C<sub>4</sub> grasses from Venezuelan savannas. *Oecologia* 67, 388–393.
- Belsky, A.L., 1994. Influences of trees on savanna productivity: tests of shade, nutrients, and tree–grass competition. *Ecology* 75 (4), 922–932.
- Belsky, A.J., Mwonga, S.M., Amundson, R.G., Duxbury, J.M., Ali, A.R., 1993. Comparative effects of isolated trees on their undercanopy environments in high- and low-rainfall savannas. *J. Appl. Ecol.* 30, 143–155.
- Breshhears, D.D., Myers, O.B., Johnson, S.R., Meyer, C.W., Martens, S.N., 1997. Differential use of spatially heterogeneous soil moisture by two semiarid woody species: *Pinus edulis* and *Juniperus monosperma*. *J. Ecol.* 85, 289–299.
- Brouwer, R., 1983. Functional equilibrium: sense or nonsense? *Neth. J. Agric. Sci.* 31, 335–348.
- Ciret, C., Polcher, J., Le Roux, X., 1999. An approach to simulate the phenology of savanna ecosystems in the LMD general circulation model. *Glob. Biogeochem. Cycles* 13, 603–622.
- Coughenour, M.B., 1994. Savanna-Landscape and regional ecosystem model, documentation. Fort Collins, Colorado State University, pp. 47.
- Cruz, P., 1997. Effect of shade on the growth and mineral nutrition of a C<sub>4</sub> perennial grass under field conditions. *Plant Soil* 188, 227–237.
- De Jong, K., 1983. Research on the water balance in a savannah ecosystem. A Study for Two Soil Types at Lamto, Ivory Coast Internal Report, ENS, pp. 73.
- Dewar, R.C., Medlyri, B.E., McMurtrie, R.E., 1998. A mechanistic analysis of light and carbon use efficiencies. *Plant Cell Env.* 21, 573–588.
- Durand, J.L., Lemaire, G., Gosse, G., Chartier, M., 1989. Analyse de la conversion de l'énergie solaire en matière sèche par un peuplement de (*Medicago sativa* L.) soumis à un déficit hydrique. *Agronomie* 9, 599–607.
- Eagleson, P.S., Segarra, R.L., 1985. Water-limited equilibrium of savanna vegetation systems. *Water Resour. Res.* 21 (10), 1483–1493.
- Gauthier, H. 1993. Echanges radiatifs et production primaire dans une savane humide d'Afrique de l'Ouest (Lamto-Côte d'Ivoire). Master Thesis, CESR University Paul Sabatier Toulouse, pp. 37.
- Gignoux, L., Menaut, L.C., Noble, L.R., Davies, I.D., 1996. A spatial model of savanna function and dynamics: model description and preliminary results. In: Prins, H.H.T., Brown, N. (Eds.), *Dynamics of Tropical Communities, the 37th Symposium of the British Ecological Society*. Blackwell, Oxford, pp. 361–383.
- Howard, S.B., Ong, C.K., Black, C.R., Khan, A.A.H., 1997. Using sap flow gauges to quantify water uptake by tree roots from beneath the rooting zone in agroforestry systems. *Agrofor. Syst.* 35, 15–29.
- Isichei, A.O., Muoghalu, J.L., 1992. The effects of tree canopy cover on soil fertility in a Nigerian savanna. *J. Trop. Ecol.* 8, 329–338.
- Jackson, L.E., Strauss, R.B., Firestone, M.K., Bartolome, J.W., 1990. Influence of tree canopies on grassland productivity and nitrogen dynamics in deciduous oak savanna. *Agric. Ecosyst. Environ.* 32, 89–105.
- Jarvis, P.G., 1976. The interpretation of the variations in leaf water potential and stomatal conductance found in canopies in the field. *Phil. Trans. R Soc. Lond. B* 273, 593–610.
- Jeltsch, R., Milton, S.L., Dean, W.J.R., Van Rooyen, N., 1996. Tree spacing and coexistence in semi-arid savannas. *J. Ecol.* 84, 583–595.
- Joffre, R., Rambal, S., 1988. Soil water improvement by trees in the rangelands of southern Spain. *Acta Oecol. (Oecol. Plant.)* 9 (4), 405–422.
- Knoop, W.T., Walker, B.H., 1985. Interactions of woody and herbaceous vegetation in a southern african savanna. *J. Ecol.* 73, 235–253.
- Korzukhin, M.D., Ter-Mikaelian, M.T., 1996. An individual tree-based model of competition for light. *Ecol. Model.* 79, 221–229.
- Landsberg, J.J., Waring, R.H., 1997. A generalised model of forest productivity using simplified concepts of radiation-use efficiency, carbon balance and partitioning. *For. Ecol. Manag.* 95, 209–228.
- Le Provost, E., 1993. Structure et fonctionnement de la strate herbacée d'une savane humide (Lamto, Côte d'Ivoire). Master Thesis, University Paris, pp. 38.
- Le Roux, X. 1995. Etude et modélisation des échanges d'eau et d'énergie sol-végétation atmosphère dans une savane humide (Lamto, Côte d'Ivoire). Ph.D. Thesis, University Paris, pp. 203.
- Le Roux, X., Bariac, T., Mariotti, A., 1995. Spatial partitioning of the soil water resource between grass and shrub components in a West African humid savanna. *Oecologia* 104, 147–155.
- Le Roux, X., Bariac, T., 1998. Seasonal variation in soil, grass and shrub water status in a West African humid savanna. *Oecologia* 113, 456–466.
- Le Roux, X., Polcher, J., Menaut, L.C., Monteny, B.A., 1994. Radiation exchanges above West African moist savannas: seasonal patterns and comparison with a GCM simulation. *J. Geophys. Res.* 99 (112), 25 857–25 868.

- Le Roux, X., Tuzet, A., Zurfluh, O., Gignoux, L., Perrier, A., Monteny, B.A., 1996. Modélisation des interactions surface/atmosphère en zone de savane humide. In: Hoepffner, M., Lebel, T., Monteny, B. (Eds.), *Interactions Surface Continentale/Atmosphère: l'expérience HAPEX-SAHÉL*. ORSTOM Editions, pp. 303–317.
- Le Roux, X., Gauthier, H., Bégué, A., Sinoquet, H., 1997. Radiation absorption and use by humid savanna grassland: assessment using remote sensing and modelling. *Agric. For. Meteorol.* 85, 117–132.
- Le Roux, X., Grand, S., Dreyer, E., Daudet, F.A., 1999. Parameterisation and testing of a biochemically based photosynthesis model for walnut (*Juglans regia*) trees and seedlings. *Tree Physiol.* 19, 481–492.
- Littleboy, M. and McKeon, G.M., 1997. Evaluating the risks of pasture and land degradation in native pastures in Queensland — Appendix 2 — Subroutine GRASP: grass production model. Indooroopilly: Rural Industries Research and Development Corporation.
- Medina, E., 1982. Physiological ecology of neotropical savanna plants. In: Huntly, B.J., Walker, B.H. (Eds.), *Ecology of Tropical Savannas*, pp. 308–335.
- Medina, E., Francisco, M., 1994. Photosynthesis and water relations of savanna tree species differing in leaf phenology. *Tree Physiol.* 14, 1367–1381.
- Menaut, J.C., 1974. Chutes de feuilles et apport au sol de litière par les ligneux dans une savane préforestière de Côte d'Ivoire. *Bull. d'Ecol.* 5, 27–39.
- Menaut, J.C., César, J., 1979. Structure and primary productivity of Larrito savannas, Ivory Coast. *Ecology* 60, 1197–1210.
- Monteith, J.L., 1972. Solar radiation and productivity in tropical ecosystems. *J. Appl. Ecol.* 2, 747–766.
- Monteith, J.L., 1977. Climate and the efficiency of crop production in Britain. *Phil. Trans. R Soc. Lond.* 281, 274–277.
- Moon, P., Spencer, D.E., 1942. Illumination from a non-uniform sky. *Trans. Illum. Eng. Soc.* 37, 707–712.
- Mordelet, P., 1993. Influence des arbres sur la strate herbacée d'une savane humide (Lamto, Côte d'Ivoire). PhD. Thesis, University Paris 6, pp. 150.
- Mordelet, P., Menaut, L.C., 1995. Influence of trees on above-ground production dynamics in a humid savanna. *J. Veg. Sci.* 6, 223–228.
- Mordelet, P., Abbadie, L., Menaut, J.C., 1993. Effects of tree clumps on soil characteristics in a humid savanna of West Africa (Lamto Côte d'Ivoire). *Plant Soil* 153, 103–111.
- Ozsisik, N.M., 1981. *Radiative Transfer*. Wiley, New York, p. 575.
- Pacala, S.W., Deutschman, D.H., 1995. Details that matter: the spatial distribution of individual trees maintains forest ecosystem function. *Oikos* 74, 357–365.
- Parton, W.J., 1996. The CENTURY model. In: Powlson, D.S., Smith, P., Smith, J.U. (Eds.), *Evaluation of soil organic matter models*. Springer-Verlag, Berlin, pp. 283–294.
- Rhoades, C.C., 1997. Single-tree influences on soil properties in agroforestry: lessons from natural forest savanna ecosystems. *Agrofor. Syst.* 35, 71–94.
- SAS Institute, 1990. *SAS/STAT user's guide*, SAS institute, Cary.
- Scholes, R.J., Archer, S.R., 1997. Tree-grass interactions in savannas. *Annu. Rev. Ecol. Syst.* 28, 517–544.
- Scholes, R.J., Hall, D.O., 1996. The carbon budget of tropical savannas, woodlands and grasslands. In: Hall, D.O., Breymer, A.I., Mellilo, J.M., Agren, G.I. (Eds.), *Global Change: Effects on Coniferous Forests and Grasslands*, SCOPE. Wiley, New York, pp. 69–100.
- Schulze, E.D., 1994. Relationships among stomatal conductance, carbon assimilation rate, and plant nitrogen nutrition: a global ecology scaling exercise. *Annu. Rev. Ecol. Syst.* 25, 629–660.
- Simoes, M., Baruch, Z., 1991. Responses to simulated herbivory and water stress in two tropical C<sub>4</sub> grasses. *Oecologia* 88, 173–180.
- Sinoquet, H., Bonhomme, R., 1992. Modeling radiative transfer in mixed and row intercropping systems. *Agric. For. Meteorol.* 62, 219–240.
- Sinoquet, H., Le Roux, X., Améglio, T., Daudet, F.A., 2000. Modélisation de la distribution spatiale du microclimat lumineux, de la transpiration et de la photosynthèse application à un arbre isolé. In: Maillard, P., Bonhomme, R. (Eds.), *Fonctionnement des Peuplements Végétaux sous Contraintes Environnementales*. INRA Editions, Série Les Colloques, Paris, pp. 185–199.
- Solbrig, O., Menaut, J.C., Mentis, M., Shugart, H.H., Stott, P., Wigston, D., 1990. Savanna modelling for global change. *Biol. Int.* 24, 3–45.
- Stuart-Hill, G.C., Tainton, N.M., 1989. The competitive interaction between *Acacia karroo* and the herbaceous layer and how it is influenced by defoliation. *J. Appl. Ecol.* 26, 285–298.
- Sueur, J., 1995. Comparaison des échanges gazeux foliaires de différents génotypes d'une graminée de savane (*Hyparrhenia diplandra*). Master Thesis, ENS Lyon.
- Tournebize, R., Sinoquet, H., Bussière, F., 1996. Modelling evapotranspiration partitioning in a shrub/grass alley crop. *Agric. For. Meteorol.* 81, 255–272.
- Ullman, I., 1985. Diurnal courses of transpiration and stomatal conductance of sahelian and saharian acacias in the dry season. *Flora* 176, 383–409.
- Walker, B.H., Ludwig, D., Holling, C.S., Peterman, R.M., 1981. Stability of semi-arid savanna grazing systems. *J. Ecol.* 69, 473–498.
- Weishampel, J.F., Urban, D.L., 1996. Coupling a spatially-explicit forest gap model with a 3-D solar routine to simulate latitudinal effects. *Ecol. Modelling* 86, 101.
- Weltzin, J.F., Coughenour, M.B., 1990. Savanna tree influence on understory vegetation and soil nutrients in northwestern Kenya. *J. Veg. Sci.* 1, 325–334.